Temperature-dependent remineralization in a warming ocean increases surface pCO_2 through changes in marine ecosystem composition

Joachim Segschneider[1,2] and Jørgen Bendtsen[2,3]

Received 3 July 2013; revised 6 November 2013; accepted 10 November 2013; published 3 December 2013.

[1] Temperature-dependent remineralization of organic matter is, in general, not included in marine biogeochemistry models currently used for Coupled Model Intercomparison Project Phase 5 (CMIP5) climate projections. Associated feedbacks have therefore not been quantified. In this study we aim at investigating how temperature-dependent remineralization rates ($Q_{10}=2$) in a warming ocean impact on the marine carbon cycle, and if this may weaken the oceanic sink for anthropogenic CO_2. We perturb an Earth system model used for CMIP5 with temperature-dependent remineralization rates of organic matter using representative concentration pathway (RCP)8.5-derived temperature anomalies for 2100. The result is a modest change of organic carbon export but also derived effects associated with feedback processes between changed nutrient concentrations and ecosystem structure. As more nutrients are recycled in the euphotic layer, increased primary production causes a depletion of silicate in the surface layer as opal is exported to depth more efficiently than particulate organic carbon. Shifts in the ecosystem occur as diatoms find less favorable conditions. Export production of calcite shells increases causing a decrease in alkalinity and higher surface pCO_2. With regard to future climate projections, the results indicate a reduction of oceanic uptake of anthropogenic CO_2 of about 0.2 PgC yr^{-1} toward the end of the 21st century in addition to reductions caused by already identified climate-carbon cycle feedbacks. Similar shifts in the ecosystem as identified here, but driven by external forcing, have been proposed to drive glacial/interglacial changes in atmospheric pCO_2. We propose a similar positive feedback between climate perturbations and the global carbon cycle but driven solely by internal biogeochemical processes.

Citation: Segschneider, J., and J. Bendtsen (2013), Temperature-dependent remineralization in a warming ocean increases surface pCO_2 through changes in marine ecosystem composition, *Global Biogeochem. Cycles*, *27*, 1214–1225, doi:10.1002/2013GB004684.

1. Introduction

[2] The biological pump constitutes a mechanism that transports CO_2 from the atmosphere to the ocean interior. Marine organisms fix carbon during growth, which lowers the water's pCO_2, causing a replacement flux from the atmosphere. The ocean net primary productivity (NPP) constitutes about 50 PgC yr^{-1}, i.e., half of the annual global NPP (ocean and land) of about 100 PgC yr^{-1} [*Field et al*., 1998]. For the ocean, *Field et al*. [1998] identify the subpolar areas, coastal upwelling zones, and equatorial regions as highly productive. The magnitude of the ocean-atmosphere carbon flux, however, depends not directly on the marine primary production, but on how much carbon is exported from the surface layer by sinking organisms in the form of organic or inorganic carbon compounds. In the preindustrial state, the uptake of carbon by marine biota and the return flux to the atmosphere are assumed to be in balance on a centennial time scale.

[3] Currently, about 20% of the global oceanic NPP is exported out of the surface layer as sinking particles [*Laws et al*., 2000; *Dunne et al*., 2007] or dissolved organic matter [*Hansell and Carlson*, 1998; *Hansell et al*., 2012]. In regions that exhibit highly to intermediate levels of productivity. the export production is negatively correlated with temperature, whereas the exported fraction only weakly depends on the total NPP [*Laws et al*., 2000]. Interdecadal variations in the NPP have been found to correlate inversely with sea surface temperature (SST) over large areas of the ocean, suggesting that temporal changes in upper ocean temperature may regulate ocean productivity [*Behrenfeld et al*., 2006]. Additionally, global studies of production and respiration rates in the ocean surface layer have shown a significant dependence upon temperature [*López-Urrutia et al*., 2006]. These studies suggest that remineralization of organic matter and hence export

[1]Max Planck Institute for Meteorology, Hamburg, Germany.
[2]Centre for Ice and Climate, Niels Bohr Institute, University of Copenhagen, Copenhagen, Denmark.
[3]ClimateLab, Copenhagen, Denmark.

Corresponding author: J. Segschneider, Max Planck Institute for Meteorology, Bundesstr. 53, D-20146 Hamburg, Germany. (joachim.segschneider@mpimet.mpg.de)

0886-6236/13/10.1002/2013GB004684

production on a global scale is sensitive to temperature changes in the upper ocean.

[4] It has, however, hitherto been assumed that the biological pump in the deep ocean is not, as such, directly responding to global warming. Consequently, the export of particulate organic carbon (POC) is not considered to be climate-sensitive in most state-of-the-art marine biogeochemical models but is described as a combination of fixed settling velocity and remineralization rate or a set of prescribed remineralization profiles, and these parameterizations implicitly assume that only negligible changes of, for example, temperature will occur in the surrounding environment.

[5] However, changes in temperature have been found to regulate metabolic rates of bacteria in both the terrestrial [*Davidson and Janssens*, 2006] and marine environments [*Rivkin and Legendre*, 2001; *López-Urrutia et al*., 2006] and also growth of higher trophic levels in the marine ecosystem is influenced by temperature [*Ikeda*, 1985].Therefore, sinking organic matter may be utilized more efficiently by heterotrophs and thereby remineralized higher up in the water column if temperature increases.

[6] Analyses of global temperature measurements during the last decades show not only an increase in SST, but also a significant increase of the heat content in the entire upper ocean where a main fraction of the remineralization occurs. The corresponding globally averaged temperature increase is estimated as 0.17°C in the upper 700 m during the period from 1969 to 2008 [*Levitus et al*., 2009]. Future global warming is likely to increase upper ocean temperatures much further [*IPCC*, 2007]. Due to increased remineralization, also below the euphotic zone, the export of organic carbon to the deeper ocean could potentially decrease. Feedbacks between increased ocean temperatures, reduced global carbon export, and hence higher atmospheric CO_2 levels leading to higher atmospheric temperatures could further reduce future ocean CO_2-uptake. The increased remineralization of POC, however, would also result in increased nutrient supply to the euphotic zone as a higher fraction of nutrients is remineralized at shallower depth levels. Thus, it is not straightforward to estimate the net effect on the marine carbon cycle and the ocean-atmosphere flux of carbon, and several points therefore have to be taken into account when trying to estimate variations of the biological pump in response to global warming.

[7] The impact of global warming on marine ecosystems has previously been identified in oceanic carbon cycle models where increased SST was shown to potentially impact the structure of ecosystem composition in the euphotic zone [*Sarmiento et al*., 2004a]. Changes would also result from changed circulation and nutrient distributions as climate changes [*Schneider et al*., 2008; *Steinacher et al*., 2010].

[8] Remineralization at shallower depths than present would tend to increase the total inorganic carbon (TCO_2) of the upper ocean, and thereby reduce the oceanic CO_2-uptake. Such mechanisms have been analyzed in an ocean carbon cycle model of intermediate complexity [*Matsumoto*, 2007] where centennial simulations showed that the oceanic uptake was significantly reduced in a global warming scenario when the remineralization of organic matter was dependent on temperature. A study with a global ocean biogeochemistry model similarly showed a significant sensitivity of oceanic CO_2-uptake and atmospheric pCO_2 to prescribed changes in remineralization depth [*Kwon et al*., 2009]. Temperature-induced changes in remineralization and export production during glacial periods have also been investigated with an ocean biogeochemistry model [*Chikamoto et al*., 2012] and resulted in better agreement with proxy records.

[9] Temperature-dependent remineralization of organic matter, however, is in general not yet included in marine biogeochemistry models currently used for the CMIP5 climate projection, and feedbacks associated with changed remineralization rates have therefore not been quantified. In this study we aim at investigating to what extent increased warming in the upper ocean, as it is projected for the 21st century, reduces carbon export into the ocean interior due to accelerated remineralization rates of organic matter, and how this may weaken the oceanic sink for anthropogenic carbon. The answer is not straightforward as faster remineralization will also increase nutrient concentrations and hence primary production in the euphotic layer, thus, making it difficult to predict the net effect.

[10] Here we analyze the sensitivity of the global carbon cycle to temperature-dependent remineralization rates with a 3-D temperature perturbation data set obtained from a Coupled Model Intercomparison Project phase 5 (CMIP5) scenario experiment with an Earth System Model. Results are analyzed not only with regard to export production, but also with regard to resulting shifts in the marine ecosystem that have an impact on alkalinity and hence pCO_2. In particular, we demonstrate that the changed alkalinity has a much larger impact on surface pCO_2 than the pure effect of changed export production.

2. Methods

2.1. Model Description

[11] We employ the Max-Planck-Institut-Earth System Model (MPI-ESM) exactly as used in the CMIP5 studies in the MPI-ESM-LR configuration, (where LR stands for "low resolution") [*Giorgetta et al*., 2013]. MPI-ESM consists of the atmospheric model ECHAM6 [*Stevens et al*., 2013], the land surface model JSBACH [*Reick et al*., 2013], the dynamical ocean model MPIOM [*Jungclaus et al*., 2013], and the marine biogeochemistry model HAMOCC5.2 [*Maier-Reimer et al*., 2005; *Ilyina et al*., 2013]. The model components are coupled using the OASIS3 coupler [*Valcke et al*., 2003]. Using a fully coupled ESM, which is a fairly heavy computational model for our analysis, allows us to compare our results to the MPI-ESM CMIP5 piControl-LR experiment (referred to as the reference case below), since our model experiment has exactly the same physical conditions, and to better estimate the relevance of the effect in the framework of current climate projections. Note that both experiments are performed with fixed preindustrial atmospheric pCO_2 as prescribed by the CMIP5 protocol. Since we use the MPI-ESM in its standard setup for CMIP5, which is described in fair detail in the above references, we will describe only the biogeochemical components of HAMOCC which are relevant for this study, i.e., the marine biology and the remineralization of organic material.

[12] The marine biology is represented by a "nutrient phytoplankton zooplankton detritus" (NPZD) model. The nutrients considered are nitrate, phosphate, iron, and silicate. HAMOCC utilizes one phytoplankton and one zooplankton group and distinguishes between particulate organic carbon

(POC) and dissolved organic carbon (DOC). To determine export production of organic carbon, the formation of detritus is computed from mortality of phytoplankton and zooplankton and fecal pellet production by zooplankton in a first step. Then, to compute the contribution of $CaCO_3$ shell formation and dissolution to alkalinity changes, the export production of opal producers (like diatoms) and calcite producers (like coccolithophores) is computed. Here the preferential formation of opal shells is assumed as long as sufficient silicate is available [e.g., *Lochte et al*., 1993; *Harrison*, 2000, and references therein]. The opal export production is first computed as a fraction (δ) of the export production of detritus depending on the available silicate (Si) with a half saturation constant (K_{Si}) of 1×10^{-6} kmol m^{-3} and limited such that it can only use half of the available silicate per time step (0.1 day), i.e., $\delta = Si/(Si + K_{Si})$. The remaining part, i.e., $1-\delta$, is attributed to the formation of calcite shells, and alkalinity is updated accordingly. More details are given in *Ilyina et al*. [2013, (see their equations (6), (12), and (14)]. Detritus, biogenic opal, and calcium carbonate are exported to depth with their respective settling velocities (5 m d^{-1} for detritus and 30 m d^{-1} for both opal and calcite shells.

[13] The remineralization of POC occurs with a fixed remineralization rate (0.025 d^{-1}). DOC is remineralized with a rate of 0.004 d^{-1} and advected and diffused with the current fields. For both, remineralization takes place in all model layers from the surface to the sea floor, i.e., including the euphotic zone, as long as sufficient oxygen is available. In oxygen poor water, denitrification of POC is simulated with a rate of 0.0025 d^{-1}. The remineralization of opal is weakly depending on temperature ($0.001 \times (T + 3°C)$ d^{-1}). The dissolution of calcite depends on the saturation state of the ambient water, which is separately calculated depending on temperature, salinity, and carbonate ion concentration. Approximate dissolution *e*-folding depths are 1000 m for POC and 4000 m for biogenic opal. For calcite, the scale is much more variable, ranging between 1000 m in the equatorial Pacific and 3000 m in the North Pacific.

2.2. Perturbation of the Remineralization Rate

[14] First, we extract the three-dimensional temperature anomaly field averaged over the last decade of the 21st century from the CMIP5 RCP8.5 scenario experiment. In a sensitivity model experiment, we apply this temperature increase by perturbing remineralization rates of organic carbon with a Q_{10} of 2 based on temperature anomalies. The physical conditions (e.g., temperature, circulation, ice cover, atmosphere, and land biosphere) are exactly as in the CMIP5 control experiment (piControl-LR), and any changes in the carbon cycle variables must originate from the changed remineralization rates.

[15] We therefore are in a position to analyze the impact of temperature-dependent remineralization on the carbon cycle without any other changes. We analyze, in particular, the ocean-atmosphere carbon flux, changes in nutrient distribution, and changes in the ecosystem structure that result from changed remineralization. We do not attempt to provide a transient estimate of the impact of temperature-dependent remineralization in the sense of a CMIP5 scenario, but rather aim at singling out the effect of temperature-dependent remineralization in a first step. Changes of the physical system and a transient CO_2 scenario would make it rather difficult, if not impossible, to separate the effect of temperature-dependent remineralization.

[16] In our experiment, we therefore perturb the remineralization rate (r) rather than change its absolute value. This assumes that the current rate (r_0) is in equilibrium with preindustrial climate. The change of organic carbon (OC) in the model is then described as:

$$\frac{\partial OC}{\partial t} + A(OC) + w_s \frac{\partial OC}{\partial z} = D(OC) - r(\theta)OC + S(OC) \quad (1)$$

where t is time, A is the advection operator, w_s is the settling velocity (it is only nonzero for POC), z is depth, D is the turbulent diffusion operator, $r(\theta)$ is the remineralization rate dependent on temperature (θ) and S is the source term of organic carbon.

[17] It is assumed that the temperature dependence $r(\theta)$ of the remineralization rate can be described as follows:

$$r(\theta) = r_0 Q_{10}^{\frac{\theta-\theta_0}{10}} \quad (2)$$

where Q_{10} is the rate change for a 10 K temperature increase and θ_0 is a reference temperature. The temperature sensitivity has been determined in several studies [*Bendtsen et al*., 2002; *Lomas et al*., 2002; *López-Urrutia et al*., 2006] and, in general, it has been found to vary around a value of 2–3. Here we apply a low global value of $Q_{10} = 2$ and consider this as a conservative estimate of the temperature sensitivity.

[18] We assume that the temperature field in the reference simulation is represented by the temporally and spatially varying temperature field (θ_r), and the local remineralization rate would then be given by equation (2) as $r(\theta_r)$.This rate is actually constant in the reference simulation, but the equation could still be valid if either r_0 or θ_0 varies in space and time. However, the sensitivity experiment only considers the variation due to local temperature changes and therefore these values will not enter the final perturbation experiment where the temperature anomaly ($\Delta\theta$) is defined locally and varies in space and time.

[19] According to equation (2), the remineralization rate at the perturbed temperature can then be calculated as follows:

$$r(\theta_r + \Delta\theta) = r(\theta_r) Q_{10}^{\frac{\Delta\theta}{10}} \quad (3)$$

where $r(\theta_r)$ is the applied (constant) remineralization rate in the reference simulation. The perturbed remineralization rate is thereby determined by the Q_{10} factor, and the spatially and temporally variable temperature change ($\Delta\theta$) in the sensitivity experiment compared to the reference case.

2.3. Applied Fields of Temperature Changes ($\Delta\theta$)

[20] In order to obtain a representative estimate of the expected temperature changes at the end of the 21st century, we analyze model results from the CMIP5 MPI-ESM-LR RCP8.5 scenario experiment. RCP8.5 represents a scenario on the high end of expected temperature change over the 21st century. We average the temperature anomalies over the years 2090–2099 and 1860–1869 in order to average out interannual variability, but retain the monthly averaged fields and thereby the seasonal cycle of the anomalies. By subtracting the 1860–1869 from the 2090–2099 temperatures, we get, as adequately as possible, a field of temperature

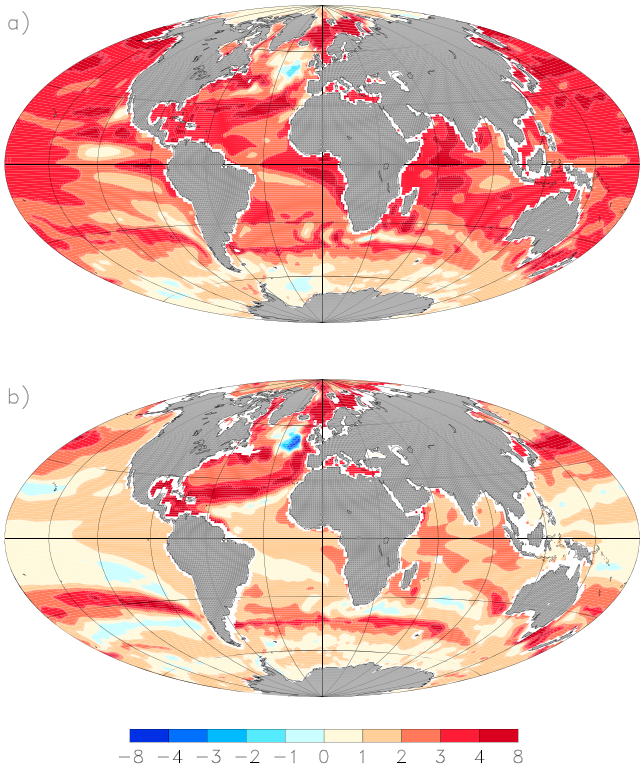

Figure 1. Temperature difference (°C) between the decadal averages of year 2090–2099 and 1860–1869 in the RCP8.5 simulation and the historical MPI-ESM-LR climate change simulation. The temperature difference is averaged between (a) 0–100 m and (b) 100–400 m depth.

anomalies that represent the oceanic warming by the end of the 21st century. These temperature anomaly fields will impact locally varying growing seasons as well as the timing of remineralization following plankton blooms.

3. Results and Discussion

[21] In the following, we will discuss changes of the sensitivity experiment, where temperature anomalies are included in the calculation of the remineralization rates, with respect to the corresponding identical years of CMIP5 experiment piControl-LR. We use the years 1850–1950 from piControl-LR and run the sensitivity experiment over the same 100 years. Thus, the physical state in both experiments is identical. For the analysis, differences are then averaged over the last 10 years of the experiments.

3.1. Temperature Changes

[22] The temperature anomaly at the end of the 21st century under RCP8.5 forcing is shown in Figure 1 for (a) the upper 100 m and (b) averaged from 100–400 m depth as annual average over the years 2090–2099. For the upper 100 m, in most regions of the ocean, a warming of 3–4 K is shown, with some localized regions of warming of up to 8 K, in particular, in the northern hemisphere. There are also regions where the temperature increase is much weaker, most notably in the Southern Ocean but also in the North Atlantic where even a small cooling occurs. The latter is caused, in the MPI-ESM-LR, by cloud feedback processes, i.e., increased cloud cover and therefore a localized cooling [T. Mauritsen, personal communication, 2012]. Between 100 m and 400 m, the warming is less marked, as expected, but nevertheless as large as 1–2 K over large regions, and a stronger warming is simulated in the North Atlantic (up to 6 K). The cold spot (Figure 1a) is even more prominent below the surface layer, and the cooling is more than 2 K. So while a warmer atmosphere leads to a heating of the ocean, this heating is not uniform, and internal processes, such as increased stratification and altered circulation, as well as external processes, such as locally increased cloud cover, result in a complex pattern of the temperature anomaly. This is of particular relevance since the remineralization of organic matter happens in localized areas. Regions of high marine production and strong projected temperature changes are most relevant for the impact of temperature-dependent remineralization on the carbon cycle. These are mainly the equatorial upwelling regions and the North Atlantic, whereas the Southern Ocean is likely to be less affected due to the smaller projected temperature increase.

[23] In the next step of the analysis, we examine the heating at greater depths using a north-south section of zonally averaged temperature anomalies and sea water density for the upper 1000 m of the global ocean (Figure 2). In particular, in regions with steep isopycnals, the temperature signal penetrates down to several hundred meters, such as in the Southern Ocean and in the North Atlantic, where a warming of more than 2 K is projected at 1000 m depth. A significant heating of 2–4 K down to about 300–500 m depth is seen below the subtropical gyres, whereas the equatorial area shows a heating of 1–2 K down to about 500 m depth. In general, there is a correspondence between the sloping isopycnals and the temperature anomalies, showing that subduction of temperate surface water masses into the upper main thermocline can account for a large part of the observed heating of the upper ocean.

3.2. Impact on Nutrients

[24] In the following, we present and discuss the changes in marine biogeochemistry that arise from the perturbed remineralization rates. In general, all these changes are small compared to the background values in the control experiment. A zonally averaged section of nitrate anomalies together with isopycnals is shown for the upper 1000 m in Figure 2b. It shows, in general, increased nitrate levels in response to increased remineralization in regions where temperature increases (Figure 2a), whereas the waters are nutrient depleted below these regions. Since the physical conditions in the sensitivity experiment are identical to those of piControl-LR, this redistribution of nutrients has to have its origin in the increased remineralization. Nitrate concentrations are seen to increase by up to 1.0 μM between the surface and about 600 m depth below the subtropical gyres whereas nitrate concentrations only increase down to about 300 m in the equatorial regions. In the Southern Ocean, a region of high importance for the low-latitude supply with nutrients and hence global biological production [*Sarmiento et al.*, 2004b] nitrate concentrations decrease by up to 0.4 μM. As more nutrients are remineralized higher up in the water column, the relative importance of subantarctic mode water (SAMW, identified by $\sigma_\vartheta \sim 26.5$–$27$) for global biological production in a warmer ocean might become less important than that identified by *Sarmiento et al.* [2004b] for the present conditions.

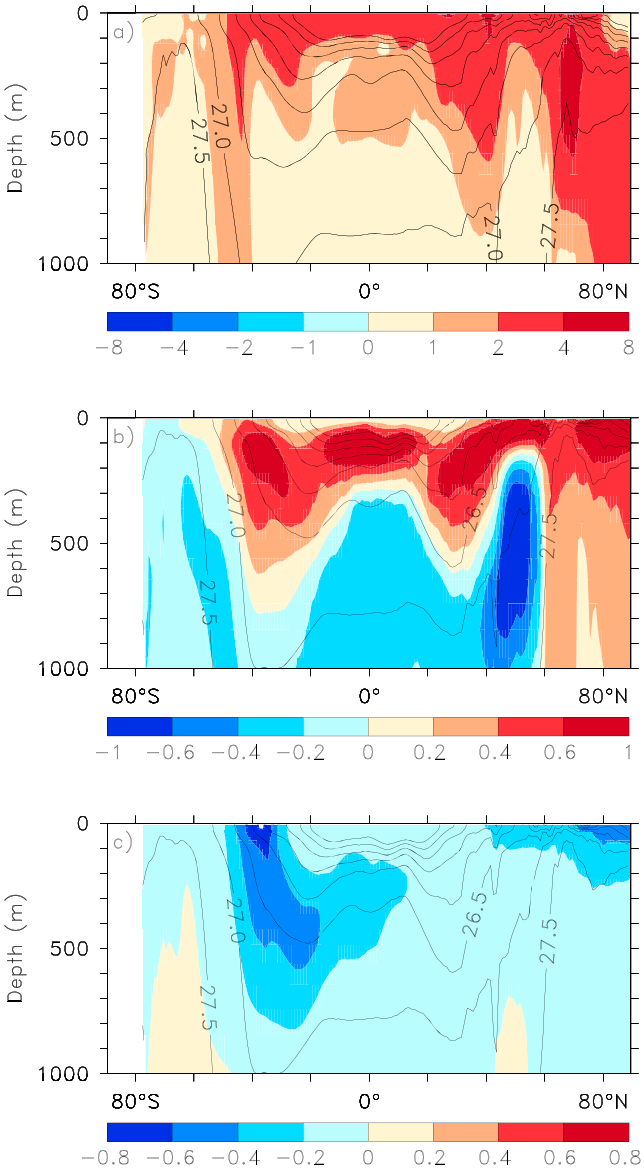

Figure 2. (a) Zonally averaged temperature difference (°C) between the decadal averages of year 2090–2099 and 1860–1869 in the RCP8.5 and historical MPI-ESM-LR climate change simulations. Zonally averaged density (σ_t) for the period 2090–2099 is contoured. (b) Zonally averaged difference of nitrate (μM) between the last 10 years of the sensitivity experiment and the respective years from the reference case, and (c) as in Figure 2b, but for silicate.

[25] The zonally averaged section of silicate (Figure 2c) shows a general decrease of silicate throughout the water column of up to −0.2 μM. A relatively large decrease is seen in the water masses associated with the Antarctic Intermediate Water of about 0.2–0.8 μM. Minor changes are seen in the Southern Ocean. The decrease of silicate can be explained by a sustained increased opal export from the surface layer which causes silicate depletion in the upper ocean, as discussed further below.

[26] As remineralization is accelerated, more nutrients are recycled within the euphotic layer (0–100 m), where they can be utilized by marine biota. The net effect of increased remineralization, increased marine production, and changed export determines the new nutrient levels. To estimate this, horizontal maps of nutrient anomalies in the euphotic zone are shown in Figure 3 for nitrate and silicate. From Figure 3a we find a generally increased level of nitrate in the upper 100 m. Negative anomalies such as simulated in the Southern Ocean around Antarctica and localized off the west coast of the Americas can occur in coastal regions if strong horizontal currents and upwelling coexist: Here near coastal waters are replaced by nutrient depleted subsurface waters as more remineralization occurs in shallower waters. For silicate, there is a general depletion in the euphotic zone (Figure 3b), and in particular the subantarctic frontal zone shows a relatively large decrease of up to 2 μM.

3.3. Primary Production and Export Fluxes

[27] To explore this further, we show in Figure 4 the distributions of anomalies for (a) integrated primary production, (b) export of POC at 90 m depth, (c) export of $CaCO_3$ at 90 m depth, and (d) the export of opal at 90 m depth.

[28] Primary production increases significantly in low latitudes, and in particular along the equator, the primary production increases by about 60–90 g C m^{-2} yr^{-1}, whereas smaller changes are seen at high latitudes (Figure 3a). In the subtropical gyres, changes in production remain small in absolute numbers even though the increase in nutrients is relatively large compared to the low local background values. Thus, the largest increase in production occurs in a belt from 15°S to 20°N. Changes in export production of organic matter (Figure 4b) result from a combination of the

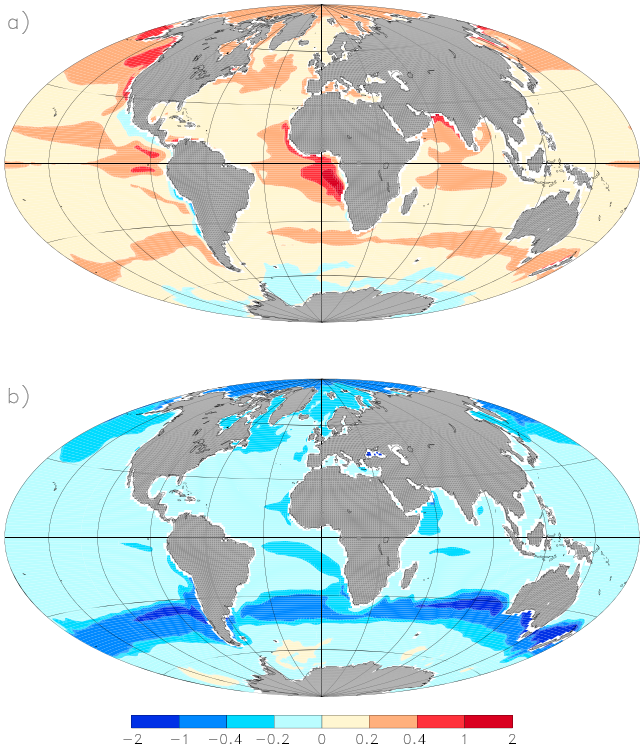

Figure 3. Horizontal maps of differences of (a) nitrate and (b) silicate (μM) between the decadal average over years 91–100 of the sensitivity experiment and the respective years in piControl from the reference case. The fields are averaged over the depth interval between 0 and 100 m.

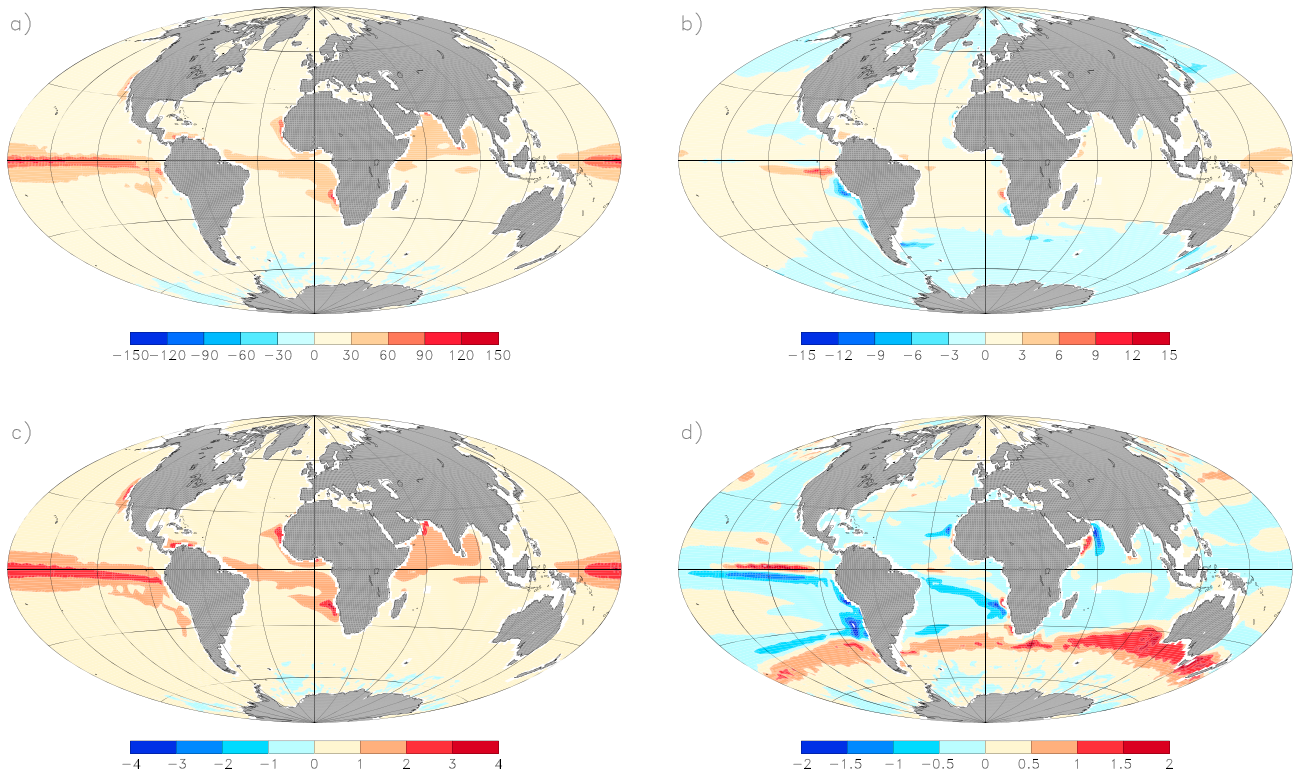

Figure 4. Horizontal maps of changes in (a) integrated primary production (g C m^{-2} yr^{-1}), (b) export of detritus at 90 m (g C m^{-2} yr^{-1}), (c) export of $CaCO_3$ at 90 m (g C m^{-2} yr^{-1}), and (d) export of opal at 90m (g Si m^{-2} yr^{-1}). The distributions are differences between the decadal average over years 91–100 of the sensitivity experiment and the reference case.

changed primary production and the changed remineralization of POC. The net result in our simulation is a slight increase in low to midlatitudes and a small decrease in high latitudes. Some localized maxima of an increase of up to 9 g C m^{-2} yr^{-1} show up in the eastern equatorial Pacific and in the Benguela upwelling system. In summary, this indicates that the major part of the increased primary production is remineralized within the euphotic layer.

[29] The changes in primary production are more directly reflected by changes in $CaCO_3$ export than for POC (Figure 4c) since $CaCO_3$ dissolution remains unchanged in our experiments, and primary production is mainly increased in regions of preferential $CaCO_3$ shell formation. This is of importance as an altered $CaCO_3$ export will change the alkalinity and hence the carbonate chemistry of the surface ocean, as discussed further below.

[30] The silicate depletion of the surface ocean (Figure 3b) can be explained by increased opal export (Figure 4d) as opal is remineralized at greater depth than organic matter and the increased nitrate availability increases marine primary production. This is particularly evident at the northern boundary of the Southern Ocean.

3.5. Changes in DIC, TA, Air-Sea CO_2 Fluxes and $CaCO_3$ Sedimentation

[31] In Figure 5, we show anomalies for dissolved inorganic carbon (DIC) and total alkalinity (TA) averaged between the surface and 100 m depth, anomalies of the CO_2 flux between ocean and atmosphere, and the anomalous flux of calcite to the sediment. The latter two are shown as they describe the main escape routes of carbon from the water column in our experiment. Negative DIC anomalies (Figure 5a) are largest in the subtropical gyres (up to −20 μM). In and near the equatorial upwelling regions of the Atlantic and Pacific, anomalies are smaller. These anomalies are mirrored by anomalies in TA (Figure 5b), indicating that changes in TA, in response to shifts in the marine ecosystem, are the main driver for the loss of carbon from the water column. The largest increase of the surface CO_2 flux from the ocean is seen in the eastern boundary current systems, in the Peru/Chile upwelling area, and the Benguela and the Canary current systems. The largest increase, of up to 8 g C m^{-2} yr^{-1}, is seen in the eastern Pacific, whereas increases between 2 and 4 g C m^{-2} yr^{-1} are seen in the North Atlantic and in the subantarctic frontal zone.

[32] Sedimentation of $CaCO_3$ (Figure 5d) only to a minor extent mirrors the export of $CaCO_3$ from the surface layer (Figure 4c) because $CaCO_3$ sedimentation and preservation at the ocean bottom also depends on the depth of the calcite compensation depth. Below the productive areas in the eastern equatorial Pacific and Atlantic, the more corrosive (lower pH) deep water masses cause less $CaCO_3$ to reach the sea floor.

3.6. Changes in the Total Carbon Inventory and Fluxes

[33] To investigate the temporal behavior of the carbon cycle changes, we show time series of globally integrated carbon fluxes and inventories over the 100 year simulation period of the experiment (Figure 6). One of the striking features is the linearity of the response, with the export of

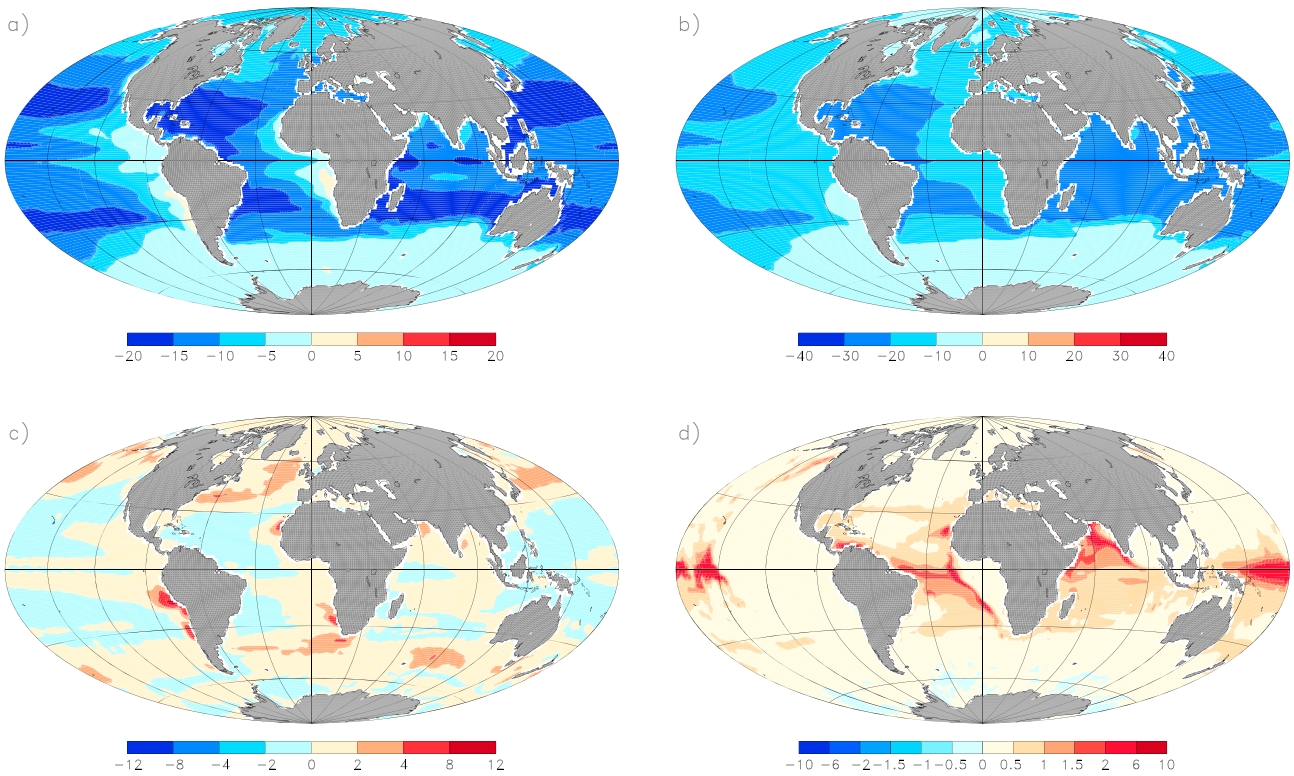

Figure 5. Horizontal maps of (a) TCO_2 averaged between 0 and 100 m depth (μM), (b) TA (μM) averaged between 0 and 100 m depth, (c) the sea-air CO_2 flux (positive upward) (g C m^{-2} yr^{-1}), and (d) the $CaCO_3$ flux to the sediment (g C m^{-2} yr^{-1}). The distributions are differences between the decadal average over years 91–100 of the sensitivity experiment and the respective years in the reference case.

POC at 90 m (dashed red curve) being the most notable exception and a modest leveling off of the opal fluxes (black dot-dashed curve) toward the end of the experiment. However, the export of POC and opal at 90 m are internal fluxes, whereas the CO_2 flux (black curve) and the sedimentation of organic (red) and inorganic (blue) carbon are fluxes through the ocean boundaries, and therefore the fluxes at 90 m show the internal adjustment to changes in vertical transports of nutrients. The increase of nutrients in the upper water column occurs over the first 10–20 years (figure not shown). The temporal behavior of the POC export can thus be explained by an initial decrease due to increased remineralization and the following increase of primary production as nutrient levels in the euphotic zone increase. Note that the flux of POC to the sea floor sediment (red curve) is still at a decreased level (i.e., negative), and hence, more nutrients are remineralized in the water column which maintains enhanced primary production (cf. Figure 4a).

[34] Figure 6 also shows that of the total loss of about 28 PgC (dashed black curve), about 18 PgC are released to the atmosphere (solid black) and 10 PgC are deposited at the sea floor in the form of $CaCO_3$ (solid blue) at the end of the experiment.

[35] The accumulated changes in marine carbon reservoirs and fluxes at the oceanic boundaries (atmosphere and sediment) are listed in Table 1. The total loss of DIC from the water column is 27.95 PgC over 100 years, i.e., about 0.3 PgC yr^{-1}. This loss is mainly the result of a flux of 18.36 PgC to the atmosphere and of 10.22 PgC to the sediment in the form of calcite. Other contributions are relatively minor: The sedimentation of organic carbon decreases by 0.88 PgC as more detritus is remineralized in the water column. The global DOC inventory increases by 0.27 PgC over the 100 years of the experiment, and the standing stocks of phytoplankton and zooplankton increase by 0.02 PgC and 0.03 PgC, respectively. Detritus in the water column

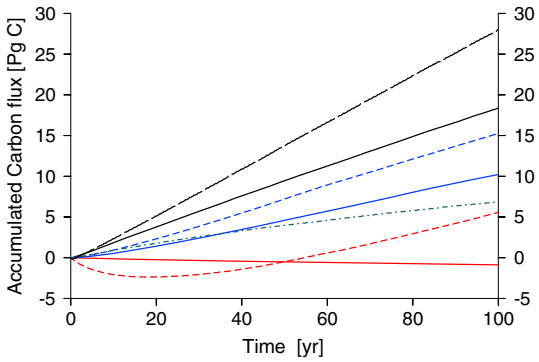

Figure 6. Changes in accumulated carbon fluxes during the 100 year long temperature sensitivity experiment. The figure shows the following: total loss from the ocean (long-dashed black), accumulated change in the air-sea CO_2 flux (solid black), the export of inorganic carbon at 90 m depth (dashed blue), sedimentation of inorganic particulate carbon (solid blue), export of organic matter at 90 m (dashed red), and sedimentation of organic matter (solid red). Changes in opal export at 90 m depth were converted into carbon units using a Si:C ratio of 20:122 (dash-dotted dark gray).

Table 1. Accumulated Changes in Marine Carbon Reservoirs and Fluxes at the Oceanic Boundaries (Atmosphere and Sediment)

Change in Global Inventories by Year 2100	Mass (PgC)	Accumulated Change in Ocean Boundary Fluxes by Year 2100	Mass (PgC)
TCO_2	−27.949	Air-sea CO_2 exchange	18.359
Detritus	−0.057	Sedimentation of $CaCO_3$	10.219
$CaCO_3$	0.051	Sedimentation of organic carbon	−0.876
Phytoplankton	0.024		
Zooplankton	0.033		
Dissolved organic carbon	0.273		
Total	−27.625		27.702

decreases by 0.06 PgC, and $CaCO_3$ increases by 0.05 PgC. These changes in boundary fluxes and ocean carbon inventories imply a mean annual CO_2 flux to the atmosphere of about 0.2 PgC yr^{-1} during the 100 year simulation and the remainder, i.e., about 0.1 PgC yr^{-1}, leaves the water column as sedimented $CaCO_3$.

[36] The almost linear decrease in the change of the total ocean carbon inventory indicates that the applied perturbation on the remineralization rates causes relatively small changes compared with the background reference fluxes in the system, as expected, and that the total impact on the ocean can be considered as a linear response on a small perturbation. However, the adjustment time is relatively long, and during a 100 year simulation, the ocean model is still responding linearly, and this reflects the long time scales associated with the ventilation of the main thermocline and vertical mixing of nutrients and carbon between the deep and surface ocean.

[37] The accumulated changes in the opal flux across 90 m are also shown for comparison (dash-dotted gray curve), and the amount of silicate is here converted into carbon units by applying the (molar) silicate:carbon (20:122) ratio in the model. The total accumulated change in the flux of 6.9 PgC at the end of the experiment corresponds to 94 Tmol Si during the 100 year simulation. This corresponds to an average change of the biogenic silica flux across 90 m of 0.94 Tmol Si yr^{-1}, and this is relatively small compared to global estimates of surface to deep ocean fluxes. The size of the opal flux is not so well constrained, but it has been estimated from a global ocean model and data analysis studies to be 148 Tmol Si yr^{-1} [*Heinze et al.*, 2003] and 105 Tmol Si yr^{-1} [*Treguer and De La Rocha*, 2013], respectively, and therefore, the simulated change of the opal flux is relatively small, corresponding to 0.5–1% change of the total surface to deep ocean opal flux.

3.7. Upper Ocean Changes in Oxygen and Denitrification

[38] The redistribution of nutrients in the upper ocean also has consequences for the production and consumption of oxygen. In a large belt in the tropical and subtropical regions, there is a weak decrease of oxygen of about 3–9 µM when averaged between 100 and 400 m depth (Figure 7a). The decrease can be explained by increased remineralization of organic matter due to the higher temperatures. In the Southern Ocean the oxygen concentrations only show minor changes, and this can be explained by the relatively small temperature changes in this area (cf. Figure 2a) and the relatively well-mixed upper ocean. In the northern Pacific the oxygen concentration between 100 and 400 m can be seen to increase by up to 12 µM. Here this depth interval is characterized by a relatively small temperature increase of about 1–2 K (cf. Figure 1b), and together with a small decrease in the export production of organic material in the area (cf. Figure 4b), the consumption of oxygen decreases slightly and this can explain the increased oxygen concentration.

[39] Note that the sensitivity experiment only considers the increased temperature change on the remineralization processes, and therefore, the decrease of surface oxygen solubility in a warmer ocean is not taken into account. If these processes were included, a larger oxygen decrease would have been simulated. However, the oxygen decrease due to remineralization processes in the tropical and subtropical oceans would enhance hypoxia and the extent of oxygen minimum zones which has been observed to already be increasing [*Stramma et al.*, 2008].

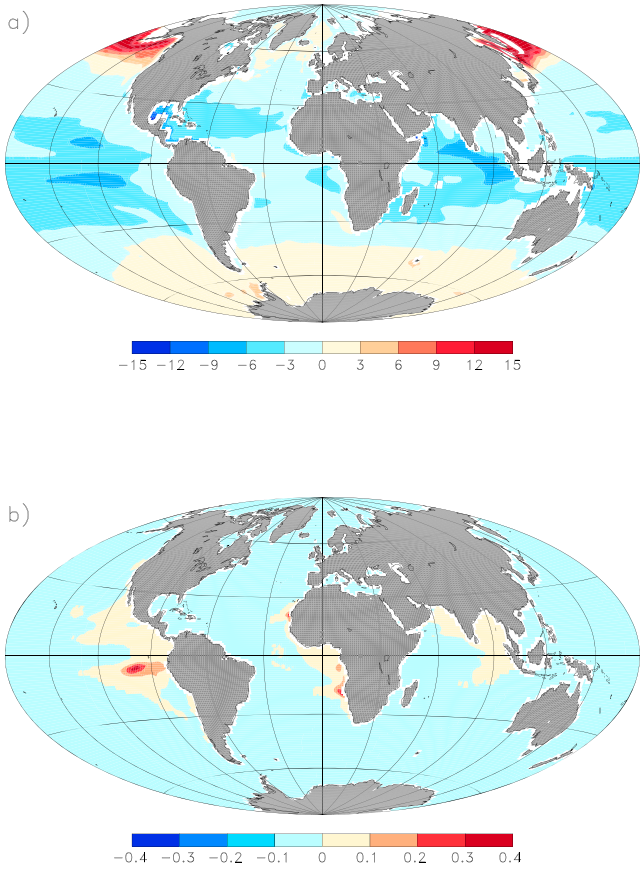

Figure 7. Depth integrated distribution of (a) change in oxygen between 100 and 400 m (µM) and (b) change in denitrification (mol N m^{-2} yr^{-1}) between the temperature sensitivity experiment and the reference case averaged over the last 10 years of the model integration.

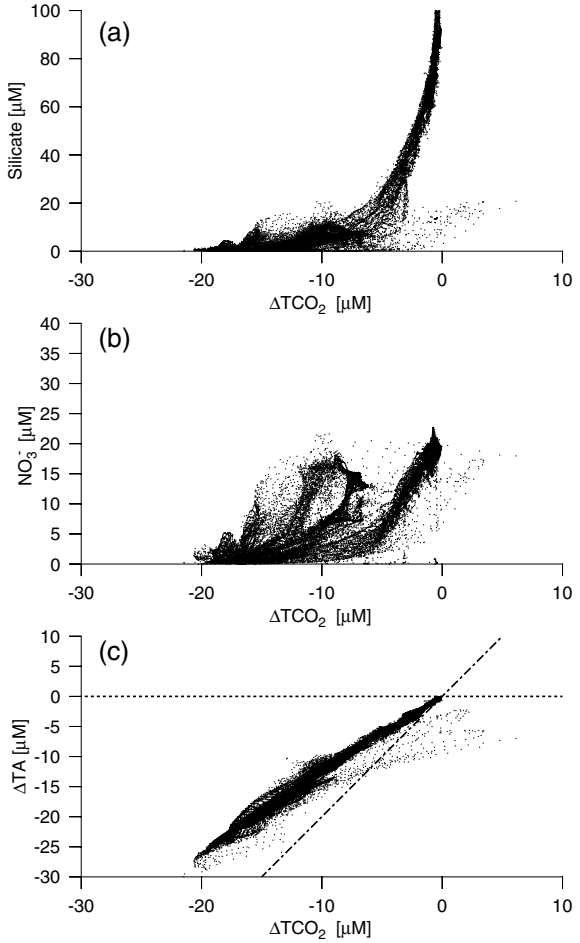

Figure 8. TCO_2 change averaged over the upper 100 m against (a) average value of minimum silicate, (b) minimum nitrate concentration, and (c) average alkalinity for all grid points above 100 m depth. Shown are the differences between temperature sensitivity experiment and the reference experiment averaged over the last 10 years of the simulation. The minimum nutrient concentrations are determined as the minimum value of the monthly averaged values in the last 10 years of the simulation. Lines corresponding to a slope of zero (dotted line) and of 2 (dash-dotted line) are indicated in Figure 8c) (see text).

[40] Increased hypoxia in the upper ocean causes increased denitrification and, in particular, in high productive upwelling regions, this is seen to increase by up to 0.4 mol N m^{-2} yr^{-1} (Figure 7b). Denitrification has the potential to enhance the feedback from remineralization processes on the oceanic CO_2 uptake by decreasing the overall nutrient level and thereby reducing the biological pump. However, denitrification may be compensated by enhanced surface nitrogen fixation, and therefore, the total significance of changes in denitrification and nitrogen fixation rates for the global carbon cycle is difficult to assess.

3.8. Mechanism of Ecosystem Change and Si Depletion

[41] In order to better understand how the mechanism described in section 3.6 operates in our model, we have plotted in Figure 8 pairs of anomalies of TCO_2 and (a) minimum silicate, (b) minimum nitrate, and (c) anomalies of TA at every grid point in the upper 100 m. The minimum concentrations of the nutrients are determined as the minimum value of the monthly averaged values during the last 10 years of the simulation period. Figure 8a shows that changes in TCO_2 occur in regions of low minimum silicate background concentrations (less than ~10 µM), i.e., where silicate limitation of diatom production occurs, and minor changes of TCO_2 is seen in areas with high silicate concentrations. Figure 8b shows that the largest changes of TCO_2 occur where nitrate levels are low, i.e., where additional nutrient supply from increased remineralization has its largest impact on primary production. If TCO_2 changes were due to uptake and production of POC only, there would be no change in surface alkalinity and TCO_2 changes would primarily be along the dotted line in Figure 8c, whereas if TCO_2 changes were due only to the formation of $CaCO_3$ shells, the associated TCO_2-TA change would follow a line with a slope of 2 (dash-dotted line in Figure 8c). However, the almost linear relationship between anomalies of TA and TCO_2 and the slope between 1 and 2 (Figure 8c) indicates that alkalinity changes are the main driver of the TCO_2 changes.

[42] This is also demonstrated by globally averaged profiles of anomalies of silicate and nitrate (Figure 9a) and TA and TCO_2 (Figure 9b). The water is silicate depleted in the upper 1000 m (solid black line), whereas nitrate (dashed line) is increased in the upper 500 m and decreased between 500 m and 2000 m depth as more POC is remineralized at shallower depth. The water column is depleted in both TCO_2 and TA in the upper ocean, whereas anomalies are positive in the deep ocean.

[43] The mechanism behind the silicate depletion and ecosystem is therefore linked to the balance between nitrate and silicate in the surface layer, and this is on longer time scales controlled by the vertical segregation and mixing of the two nutrients between the deep ocean and the euphotic zone. The increased remineralization rate due to rising temperatures leads to less transport of organic matter into the deep ocean, and it causes the concentration of nutrients and TCO_2 in the upper main thermocline to increase (Figure 10). Increased TCO_2 levels in the upper ocean would tend to increase the surface concentration of CO_2 and thereby tend to increase the ocean-to-atmosphere CO_2 flux. However, increased surface concentrations of nutrients would favor the production of diatoms over coccolithophores, due to their larger growth rate, and an increased opal production and export would follow. Because opal is sinking faster and dissolution is less influenced by rising temperatures, more silicate will gradually be exported into the deep ocean and finally the balance between ocean vertical mixing and silicate distribution would lead to a reduced influx of silicate to the surface layer. Subsequently, production of coccolithophores would tend to be favored in the silicate-depleted surface layer and uptake of carbonate ions for the formation of their $CaCO_3$-shells reduces the TA in the surface layer which would tend to increase the surface pCO_2 and thereby the ocean-to-atmosphere carbon flux.

3.9. Implications of Ecosystem Changes During Different Climatic Periods

[44] The influence from a shift in the global ecosystem structure from opal-producing diatoms to calcifying coccolithophores

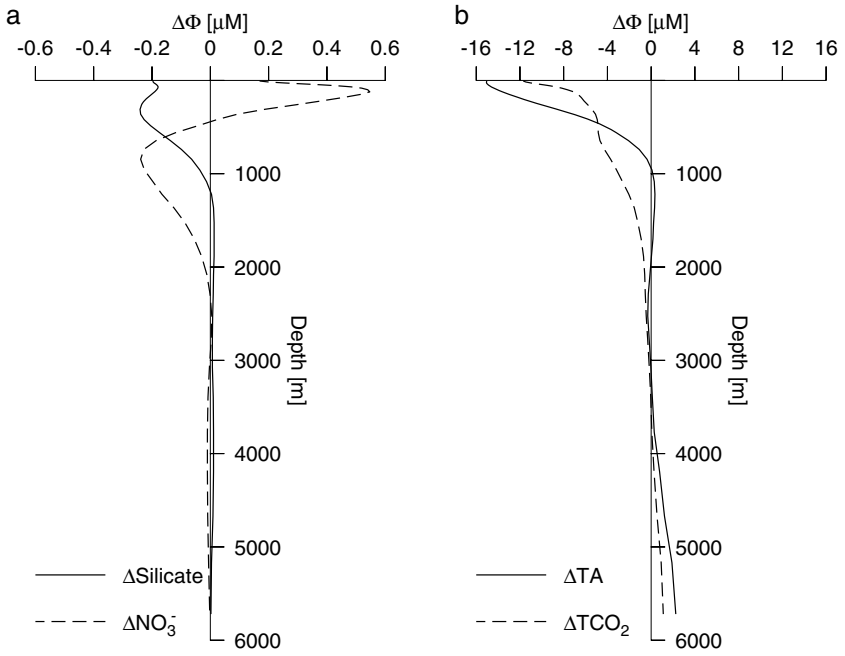

Figure 9. Globally averaged profiles of changes in (a) silicate (solid) and nitrate (dashed) and (b) TA (solid) and TCO_2 (dashed) (μM). Differences between the decadal average over years 91–100 of the sensitivity experiment and the respective years in the reference case.

was first analyzed in a simple model by *Dymond and Lyle* [1985], motivated by their findings of calcite and opal fluxes from sediment traps in the tropical Pacific. They found that increased production of calcifying organisms would tend to increase surface pCO_2 and thereby help in explaining glacial-interglacial CO_2 changes. The role of the relative amount of calcite versus organic carbon export flux (i.e., the rain ratio) was investigated further in a coupled global ocean-sediment model by *Archer and Maier-Reimer* [1994], who simulated a shift from calcifying organisms (e.g., coccolithophores) toward silicious organisms (diatoms) by varying the rain ratio accordingly, and they found that a 40% decrease of the calcite flux could explain the interglacial to glacial pCO_2 drawdown of 80 ppm. *Harrison* [2000] proposed the "silica hypothesis" where direct input of silicate, via atmospheric transports of dust, would stimulate production of diatoms, and this would imply a reduction of calcite flux from the surface layer and thereby lower surface pCO_2. This hypothesis was further elaborated in the study of *Matsumoto et al.* [2002], where the "silicic acid leakage hypothesis" was proposed and the sensitivity of the silicic acid to nitrate ratio in the uptake of diatoms to the presence of iron was included. Iron-rich environments, e.g., as expected over the Southern Ocean during glacial periods, would imply a lower Si:N uptake in the surface layer, and thereby, the excess silicate would be available for diatom production elsewhere in the ocean. They hypothesize that advection of silicate-rich subsurface water masses from the Southern Ocean could stimulate diatom production at lower latitudes. This hypothesis was supported by isotope studies of sediment cores from Antarctic sediments [*Brzezinski et al.*, 2002]. However, later sediment studies indicated that the implied ecosystem shift in the Southern Ocean

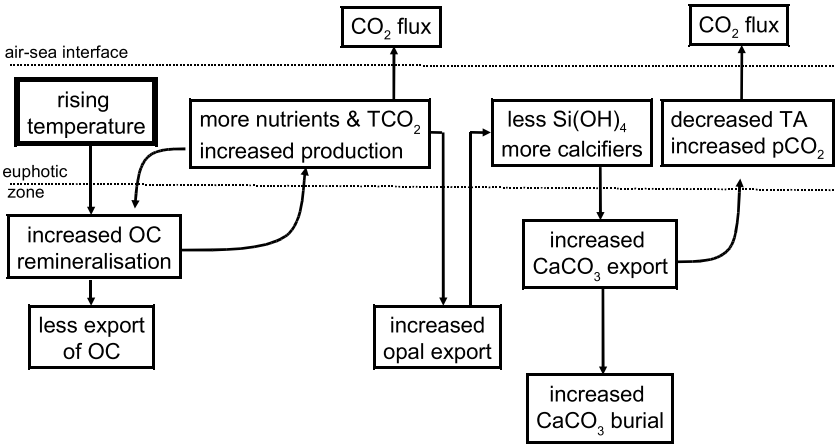

Figure 10. Conceptual flow diagram of the impact from temperature-dependent remineralization on export production and subsequent silica usage and depletion in the surface layer of the ocean (see text).

could not explain the initial pCO_2 decrease from the last interglacial to the glacial period, but sediment studies did support a major ecosystem shift from calcifying producers toward diatoms during the glacial period [*Kohfeld et al*., 2005]. These studies underline the importance of ecosystem structure for understanding long-term changes in atmospheric CO_2, and the mechanism shown here (Figure 10) can basically be explained by the principles of the silica hypothesis. As a major difference here, there is no requirement for an external input of silicate (or iron) driving the ecosystem change but rather an internal oceanic adjustment to changed nutrient distributions.

3.10. Global Warming and Positive Feedbacks

[45] In this study we focus on time scales similar to the CMIP5 experiments, i.e., roughly 100 years from now. We identified a process which is not yet presented in the current set of scenario experiments. Moreover, this process will in principle operate even after fossil fuel burning has ceased as long as temperatures remain anomalous high. The linearity of the response over the 100 simulated years suggests that a substantial loss of carbon to the atmosphere will occur over several hundred years. Unfortunately, our model system is too expensive to extend the model run until a new equilibrium is reached, so we are not in a position to state exactly for how long—and how much—additional carbon will be released to the atmosphere, potentially driving a further climate warming.

[46] *Kwon et al*. [2009] estimated the equilibrium *e*-folding time to changes in the remineralization depth to be about 500 years in an ocean-only model, and a minimum of 2000 years was found to be necessary for reaching a new equilibrium in their model. Thus, this study supports that the positive feedback from temperature-dependent remineralization may become more significant on longer time scales. *Matsumoto* [2007] applied a coupled model of intermediate complexity and was able to simulate the atmospheric pCO_2 change during 1000 years due to a similar temperature-dependent remineralization parameterization and found a somewhat smaller *e*-folding time of about 200 years. *Matsumoto* [2007] estimated an increase of atmospheric pCO_2 of about 20 ppm after the first 100 years of simulation, but this was for a stronger temperature change of 5°C, indicating a somewhat lower sensitivity than in the present study. However, the net effects from a temperature-dependent remineralization are in accordance with the results from this study.

[47] In a pioneering study, *Friedlingstein et al*. [2006] quantified the climate-carbon cycle feedback due to climate warming alone based on multimodel C4MIP experiments with a suite of ESMs. For the coupled system, they found that the feedback caused an increase of atmospheric pCO_2 by 20–100 ppm by 2100. While the major part of this feedback was attributed to the models' land components, oceanic uptake was also reduced on average by around 0.5 PgC yr^{-1} by 2100 (their Figure 1f). The reduction of 0.2 PgC yr^{-1} for 2100 due to temperature-dependent remineralization identified here had not been included in the ocean components in *Friedlingstein et al*. [2006] and will additionally decrease the oceanic uptake of anthropogenic carbon by a significant amount.

3.11. Limitations of the Study

[48] Although we employed a state-of-the-art model, it is clear that important processes that may serve to modulate the responses emphasized here were not included. For example, detrimental effects of acidification on calcite forming organisms in a high CO_2 world may counteract the shift to stronger coccolithophores production under silicate depletion and thus the increase in calcite export and accompanying alkalinity change may be damped. Also the resulting effect on settling velocity of detritus from changes in rain ratio and ballast effect is not included in our model. From the comparison of CMIP5 MPI-ESM-LR and CMIP5 MPI-ESM-MR (nominal horizontal resolution of the oceanic component 1.5° with a refinement in the North Atlantic and homogeneously 0.4°, respectively) in *Ilyina et al*. [2013], increasing the oceanic resolution to MR is unlikely to have a major impact on our results.

4. Conclusions

[49] It can first be concluded that temperature-dependent remineralization has an impact on the large-scale carbon distribution and ocean-to-atmosphere CO_2 flux which is not negligible compared to the rates of oceanic uptake of anthropogenic CO_2. The ocean-to-atmosphere CO_2 flux increases mainly in regions of high biological production indicating that increased remineralization dominates the carbon cycle changes in these areas. The net loss of oceanic carbon is almost 0.3 PgC yr^{-1}, of which 0.2 PgC yr^{-1} are released to the atmosphere during the 100 years of simulation in the experiment. The accumulated change in the ocean uptake of about 20 PgC in 100 years is a significant amount when compared to anthropogenic emissions and, in particular, compared to planned reductions in global carbon emissions. Moreover, this reduction in oceanic carbon uptake amounts to about half of the ocean carbon cycle-climate feedback identified in *Friedlingstein et al*. [2006], and will additionally reduce the oceanic carbon uptake. A further main result is that calcite export and the resulting alkalinity changes play a significant role in the carbon cycle changes. Earlier studies underline the importance of ecosystem structure for understanding long-term changes in atmospheric CO_2 based on external supply of silicate and/or iron. In our study we identify internal oceanic adjustment to changed nutrient distributions in response to changing temperature as a driver of changed ocean-atmosphere CO_2 flux. For the near future, we are aiming at performing a more comprehensive study, also including more models and potentially also forced by glacial temperature fields to investigate the impact of cooling in the near future.

[50] **Acknowledgments.** The research leading to these results was supported through EU FP7 project CARBOCHANGE "Changes in carbon uptake and emissions by oceans in a changing climate," which received funding from the European Commission's Seventh Framework Programme under grant agreement 264879. We wish to thank two anonymous reviewers for their constructive comments. Computations were carried out at Deutsches Klimarechenzentrum, Hamburg, Germany.

References

Archer, D., and E. Maier-Reimer (1994), Effect of deep-sea sedimentary calcite preservation on atmospheric CO_2 concentration, *Nature*, *367*, 260–264.

Behrenfeld, M. J., R. T. O'Malley, D. A. Siegel, C. R. McClain, J. L. Sarmiento, G. C. Feldman, A. J. Milligan, P. G. Falkowski, R. M. Letelier, and E. M. Boss (2006), Climate-driven trends in contemporary ocean productivity, *Nature*, doi:10.1038/nature0531.

Bendtsen, J., C. Lundsgaard, M. Middelboe, and D. Archer (2002), Influence of bacterial uptake on deep-ocean dissolved organic carbon, *Global Biogeochem. Cycles*, *16*(4), 1127, doi:10.1029/2002GB001947.

Brzezinski, M. A., C. J. Pride, V. M. Franck, D. Sigman, J. L. Sarmiento, K. Matsumoto, N. Gruber, G. H. Rau, and K. H. Coale (2002), A switch from $SI(OH)_4$ to NO_3-depletion in the glacial Southern Ocean, *Geophys. Res. Lett.*, *29*(12), 1564, doi:10.1029/2001GL014349.

Chikamoto, M. O., A. Abe-Ouchi, A. Oka, and S. L. Smith (2012), Temperature-induced marine export production during glacial period, *Geophys. Res. Lett.*, *39*, L21601, doi:10.1029/2012GL053828

Davidson, E. A., and I. A. Janssens (2006), Temperature sensitivity of soil carbon decomposition and feedbacks to climate change, *Nature*, *440*, 165–73.

Dunne, J. P., J. L. Sarmiento, and A. Gnanadesikan (2007), A synthesis of global particle export from the surface ocean and cycling through the ocean interior and on the seafloor, *Global Biogeochem. Cycles*, *21*, GB4006, doi:10.1029/2006GB002907.

Dymond, J., and M. Lyle (1985), Flux comparisons between sediments and sediment traps in the eastern tropical Pacific: Implications for atmospheric CO_2 variations during the Pleistocene, *Limnol. Oceanogr.*, *39*, 699–712.

Field, C. B., M. J. Behrenfeld, and J. T. Randerson (1998), Primary production of the biosphere: Integrating terrestrial and oceanic components, *Science*, *281*, 237–240.

Friedlingstein, P., et al. (2006), Climate–Carbon Cycle Feedback Analysis: Results from the C4MIP Model Intercomparison, *J. Climate*, *19*, 3337–3353, doi:10.1175/JCLI3800.1.

Giorgetta, M., et al. (2013), Climate change from 1850 to 2100 in MPI-ESM simulations for the Coupled Model Intercomparison Project phase 5, *J. Adv. Model. Earth Syst.*, *5*, 672–597, doi:10.1002/jame.20038.

Hansell, D. A., and C. A. Carlson (1998), Net community production of dissolved organic carbon, *Global Biogeochem. Cycles*, *12*, 443–453.

Hansell, D. A., C. A. Carlson, and R. Schlitzer (2012), Net removal of major marine dissolved organic carbon fractions in the subsurface ocean, *Global Biogeochem. Cycles*, *26*, GB1016, doi:10.1029/2011GB004069

Harrison, K. G. (2000), Role of increased marine silica input on paleo-pCO_2 levels, *Paleoceanography*, *15*, 292–298.

Heinze, C., A. Hupe, E. Maier-Reimer, N. Dittert, and O. Ragueneau (2003), Sensitivity of the marine biospheric Si cycle for biogeochemical parameter variations, *Global Biogeochem. Cycles*, *17*(3), 1068, doi:10.1029/2002GCB001943.

Ikeda, T. (1985), Metabolic rates of epipelagic marine zooplankton as a function of body mass and temperature, *Mar. Biol.*, *85*, 1–11.

Ilyina, T., K. D. Six, J. Segschneider, E. Maier-Reimer, H. Li, and I. Núñez-Riboni (2013), Global ocean biogeochemistry model HAMOCC: Model architecture and performance as component of the MPI-Earth System Model in different CMIP5 experimental realizations, *J. Adv. Model. Earth Syst.*, *5*, 287–315, doi:10.1002/jame.20017.

IPCC (2007), Climate change: The physical science basis, in *Contribution of Working Group I to the Fourth Assessment Report of the Intergovernmental Panel on Climate Change*, edited by S. Solomon et al., pp. 996, Cambridge Univ. Press, Cambridge, U. K., and New York.

Jungclaus, J. H., N. Fischer, H. Haak, K. Lohmann, J. Marotzke, D. Matei, U. Mikolajewicz, D. Notz, and J. S. von Storch (2013), Characteristics of the ocean simulations in MPIOM, the ocean component of the MPI-Earth System Model, *J. Adv. Model. Earth Syst.*, *5*, 422–446, doi:10.1002/jame.20023.

Kohfeld, K. E., C. Le Quéré, S. P. Harrison, and R. F. Anderson (2005), Role of marine biology in glacial-interglacial CO_2 cycles, *Science*, *308*, 74–78.

Kwon, E. Y., F. Primeau, and J. L. Sarmiento (2009), The impact of remineralization depth on the air-sea carbon balance, *Nat. Geosci.*, *2*, doi:10.1038/NGEO612.

Laws, E. A., P. G. Falkowski, W. O. Smith, H. Ducklow, and J. C. McWilliams (2000), Temperature effects on export production in the open ocean, *Global Biogeochem. Cycles*, *14*, 1231–1246.

Levitus, S., J. I. Antonov, T. P. Boyer, R. A. Locarnini, H. E. Garcia, and A. V. Mishonov (2009), Global ocean heat content 1955–2008 in light of recently revealed instrumentation problems, *Geophys. Res. Lett.*, *36*, L07608, doi:10.1029/2008GL037155.

Lochte, K., H. Ducklow, M. Fasham, and C. Stienen (1993), Plankton succession and carbon cycling at 47°N 20°W during the JGOFS North Atlantic Bloom Experiment, *Deep Sea Res., Part II*, *40*(1), 91–114.

Lomas, M. W., P. M. Glibert, F. K. Shiah, and E. M. Smith (2002), Microbial processes and temperature in Chesapeake Bay: Current relationships and potential impacts of regional warming, *Global Change Biol.*, *8*, 51–70.

López-Urrutia, Á., E. S. Martin, R. P. Harris, and X. Irigoien (2006), Scaling the metabolic balance of the oceans, *Proc. Natl. Acad. Sci. U.S.A.*, *103*, 8739–8744.

Maier-Reimer, E., I. Kriest, J. Segschneider, and P. Wetzel (2005), The Hamburg ocean carbon cycle model HAMOCC5.1. Technical description, Release 1.1. Berichte zur Erdsystemforschung, 14/2005, Max-Planck-Institut für Meteorologie.

Matsumoto, K. (2007), Biology-mediated temperature control on atmospheric pCO_2 and ocean biogeochemistry, *Geophys. Res. Lett.*, *34*, L20605, doi:10.1029/2007GL031301.

Matsumoto, K., J. L. Sarmiento, and M. A. Brzezinski (2002), Silicic acid leakage from the Southern Ocean: A possible explanation for glacial atmospheric pCO_2, *Global Biogeochem. Cycles*, *16*(3), 1031, doi:10.1029/2001GB001442.

Reick, C. H., T. Raddatz, V. Brovkin, and V. Gayler (2013), The representation of natural and anthropogenic land cover change in MPI-ESM, *J. Adv. Model. Earth Syst.*, *5*, 459–482, doi:10.1002/jame.20022.

Rivkin, R. B., and L. Legendre (2001), Biogenic carbon cycling in the upper ocean: Effects of microbial respiration, *Science*, *291*, 2398–2400.

Sarmiento, J. L., et al. (2004a), Response of ocean ecosystems to climate warming, *Global Biogeochem. Cycles*, *18*, GB3003, doi:10.1029/2003GB002134.

Sarmiento, J. L., N. Gruber, M. A. Brzezinski, and J. P. Dunne (2004b), High latitude controls of thermocline nutrients and low latitude productivity, *Nature*, *427*, 56–60.

Schneider, B., L. Bopp, M. Gehlen, J. Segschneider, T. Frölicher, F. Joos, P. Cadule, P. Friedlingstein, S. C. Doney, and M. J. Behrenfeld (2008), Spatio temporal variability of marine primary and export production in three coupled climate carbon cycle models, *Biogeosciences*, *5*, 597–614.

Steinacher, M., F. Joos, T. L. Frölicher, L. Bopp, C. Cadule, S. C. Doney, M. Gehlen, B. Schneider, and J. Segschneider (2010), Projected 21st Century decrease in marine productivity: A multi model analysis, *Biogeosciences*, *7*, 979–1005.

Stevens, B., et al. (2013), Atmospheric component of the MPI-M Earth System Model: ECHAM6, *J. Adv. Model. Earth Syst.*, *5*, 146–172, doi:10.1002/jame.20015.

Stramma, L., G. C. Johnson, J. Sprintall, and V. Mohrholz (2008), Expanding oxygen-minimum zones in the tropical oceans, *Science*, *320*, 655–658.

Treguer, P. J., and C. L. De La Rocha (2013), The world ocean silica cycle, *Annu. Rev. Mar. Sci.*, *5*, 477–501.

Valcke, S., A. Caubel, D. Declat, and L. Terray (2003), OASIS Ocean Atmosphere Sea Ice Soil User's Guide. CERFACS Tech. Rep. TR/CMGC/03/69, Toulouse, France, 85 pp.